

RESEARCH

In-flight Scalar Calibration and Characterisation of the Swarm Magnetometry Package

Lars Tøffner-Clausen^{1*}, Vincent Lesur², Nils Olsen¹ and Christopher C. Finlay¹

*Correspondence:

lastec@space.dtu.dk

¹Division of Geomagnetism, DTU Space, Technical University of Denmark, Diplomvej, Kongens Lyngby, Denmark

Full list of author information is available at the end of the article

Abstract

We present the in-flight scalar calibration and characterisation of the *Swarm* magnetometry package consisting of the absolute scalar magnetometer (ASM), the vector magnetometer (VFM), and the spacecraft structure supporting the instruments. A significant improvement in the scalar residuals between the pairs of magnetometers is demonstrated, confirming the high performance of these instruments. The results presented here, including the characterization of a Sun-driven disturbance field, form the basis of the correction of the magnetic vector measurements from *Swarm* which is applied to the *Swarm* Level 1b magnetic data.

Keywords: Geomagnetism; Magnetometer; Instrument Calibration; Satellite; *Swarm*

1

2

1 Introduction

In November 2013 the European Space Agency (ESA) launched the three *Swarm* satellites named *Alpha*, *Bravo*, and *Charlie* with the objective to provide the best ever survey of the geomagnetic field and its temporal evolution ([Friis-Christensen et al., 2006](#)). Each spacecraft carries an Absolute Scalar Magnetometer (ASM) for measuring Earth's magnetic field intensity, a Vector Fluxgate Magnetometer (VFM) measuring the direction and strength of the magnetic field, and a three-head Star TRacker (STR) mounted close to the VFM to obtain the attitude needed to transform the vector readings to an Earth fixed coordinate frame. Time and position are provided by an on-board GPS receiver. The payload also includes instruments to measure plasma and electric field parameters as well as non-gravitational acceleration. More information on the mission status after two years in orbit can be found in [Floborghagen et al. \(2016\)](#).

16

One of the purposes of the scalar magnetometer (ASM) is to provide the necessary absolute magnetic data to calibrate the vector magnetometer (VFM). For this an approach similar to that adopted for the previous satellite missions Ørsted and CHAMP was foreseen (c.f. [Olsen et al., 2003](#); [Yin and Lühr, 2011](#)) since those missions carried equivalent instrumentation. However, soon after launch of *Swarm* it became clear that the magnetic field vector measurements on all three spacecraft were contaminated by unforeseen disturbances which could not be captured by the traditional in-flight calibration methods referred to above. Furthermore, the disturbances show systematic variation which could impact or map into scientific investigations based on *Swarm* magnetic data. The light blue symbols in Fig. 1 show

26

27 time series of the *scalar residuals*, which are the difference, $\Delta F = |\vec{B}_{\text{VFM}}| - F_{\text{ASM}}$,
 28 between the modulus of the VFM data, $|\vec{B}_{\text{VFM}}|$, and the magnetic intensity mea-
 29 surements, F_{ASM} , taken by the ASM instrument. Based on experience with Ørsted
 30 and CHAMP scalar residuals with sub-nanotesla level were expected (rms value
 31 well below 0.5 nT), while for *Swarm* the scatter of the residuals was observed to
 32 reach several nT, resulting in an rms value approaching 1 nT, but crucially show-
 33 ing a very clear Local Time dependence. A task force was therefore established to
 34 investigate and mitigate the effect.

35
 36 Detailed investigations of the scalar residuals ΔF and of the ASM and VFM
 37 measurements separately indicated that:

- 38 • the vector readings of the VFM are affected by a disturbance vector field;
- 39 • the scalar readings of the ASM are much less, if at all, affected.

40 Consequently the Task Force concluded to pursue models which assume the mag-
 41 netic disturbance to be affecting the VFM measurements only. Plotting ΔF as a
 42 function of the Sun incidence angles with respect to the spacecraft, reveals system-
 43 atic features of the disturbance, as shown in Fig. 3. At the start of section 2 we
 44 provide detailed definitions of the two Sun incidence angles α and β . This supports
 45 the hypothesis that a magnetic source in the vicinity of the VFM magnetometer,
 46 with strength and direction depending on the direction to the Sun (as seen from the
 47 spacecraft), is responsible. We refer to such a disturbance field vector, that depends
 48 on the direction to the Sun, as $\delta\vec{B}_{\text{Sun}}$.

49
 50 The purpose of this article is to document the details of in-flight calibration of the
 51 *Swarm* magnetometer package, including an empirical determination and removal
 52 of the Sun driven vector disturbance field $\delta\vec{B}_{\text{Sun}}$, based on a mitigation approach
 53 proposed by Vincent Lesur ([Lesur et al., 2015](#)).

54
 55 Section 2 describes the parameterisation of the model of the Sun-driven distur-
 56 bance – in following referred to as the *characterisation* of the disturbance field
 57 – and of the *calibration* of the VFM instrument, by which means determination
 58 of its intrinsic scale factors and their dependence on time and temperature, and
 59 determination of the sensor-axis non-orthogonalities. We document the adopted
 60 Iteratively Reweighted Least Squared (IRLS) estimation approach, that includes
 61 a truncated singular value decomposition (SVD) approach to solving the inverse
 62 problem. The results obtained for *Swarm Alpha*, based on data covering the pe-
 63 riod from launch (22. November 2013) until end of June 2015 (i.e. 19 months), are
 64 presented in Section 3. Application of the scheme to data from the satellites *Bravo*
 65 and *Charlie* resulted in similar levels of residual improvement and statistics, and
 66 the estimates of the Sun driven disturbance $\delta\vec{B}_{\text{Sun}}$ show generally similar behaviour
 67 and structural features as found for *Swarm Alpha*, although there are also some
 68 differences. Finally, Section 4 summarizes the findings and provides perspectives
 69 regarding further improvements of the method.

71 2 Characterisation and Calibration with Scalar Residuals

72 The Sun incidence angles α and β are crucial in our approach to *characterise* the
 73 scalar residual. To clarify, in Fig. 2 we illustrate the definition of these angles with
 74 respect to the spacecraft and the Sun position. α is the azimuth in the spacecraft
 75 x-z plane (nominally the orbit plane) and β is the “elevation” out of the x-z plane
 76 positive towards *left* (looking in the nominal flight direction; i.e. positive *opposite*
 77 the spacecraft *y* axis). ~~Examples of values for α and β for particular Sun positions~~
 78 ~~are: Considering how these angles vary over orbits of the *Swarm* spacecraft, we find~~
 79 ~~the angle α varies rapidly: from 0° to 360° within one orbit (i.e. within ≈ 90 minutes)~~
 80 ~~while the other angle, β , varies more slowly (by $\approx 1.5^\circ$ in one day).~~

- 81 • $\beta = +90^\circ$: Sun directly from $-y$ (i.e. from the left during nominal flight)
- 82 • $\beta = -90^\circ$: Sun directly from $+y$ (i.e. from the right)
- 83 • $\beta = 0^\circ, \alpha = 0^\circ$: Sun directly from $+x$ (i.e. from the front)
- 84 • $\beta = 0^\circ, \alpha = +90^\circ$: Sun directly from $-z$ (above)
- 85 • $\beta = 0^\circ, \alpha = +180^\circ$: Sun directly from $-x$ (i.e. from the back – slightly above
 86 the boom)

87 Considering how these angles vary over orbits of the *Swarm* spacecraft during nom-
 88 inal flight, we find that α varies rapidly: from 360° down to 0° within one orbit (i.e.
 89 within ≈ 90 minutes) while β , varies slowly up and down typically by $\approx 1.25^\circ$ in
 90 one day (for *Alpha* and *Charlie*, 1.20° for *Bravo*).

91
 92 Although the observed scalar residuals clearly vary with the Sun incidence angles
 93 α and β (see Fig. 3) there is no direct mapping of ΔF in terms of these parameters.
 94 This is a consequence of the scalar residuals $\Delta F \approx \delta \vec{B}_{\text{Sun}} \cdot \vec{b}_0$ being the projection
 95 of the magnetic disturbance vector $\delta \vec{B}_{\text{Sun}}$, onto the unit vector \vec{b}_0 of the ambient
 96 magnetic field direction (Earth’s main field). The former is oriented relative to
 97 the spacecraft while the latter is oriented relative to Earth, which results in the
 98 variations with the spacecraft local time (captured by β) as seen in Fig. 3. The
 99 spacecraft local time changes by 12 hours (corresponding to a change in β by 180°)
 100 within approximately $4\frac{1}{2}$ months.

101
 102 To account for the projection on to the ambient field, we consider a *vector* mag-
 103 netic disturbance $\delta \vec{B}_{\text{Sun}}(\alpha, \beta)$, with each component depending individually on the
 104 Sun incidence angles. Mathematically, we describe each component of the distur-
 105 bance field vector by a spherical harmonic expansion in α and β i.e. we consider
 106 three independent spherical harmonic expansions in all.

107
 108 This model *characterizing* the Sun-driven disturbance is co-estimated together
 109 with a model of the temporal evolution of the VFM sensitivity and an adjustment
 110 of the pre-flight estimated non-orthogonality angles of the VFM sensor. For this
 111 we perform a *scalar calibration* via a least squares fit, minimizing the discrepancy
 112 (ΔF) between the **fully calibrated and corrected** measurements from **the** ASM and
 113 the modulus of the vector measurements from the VFM after our model has been
 114 applied. Huber weights are used iteratively to eliminate the effect of anomalous
 115 measurements (“outliers”) on the estimated models.

117 2.1 Model Parameterisation

118 As outlined above, our model characterizing the Sun-driven disturbance vector
 119 $\delta\vec{B}_{\text{Sun}}$ consists of three spherical harmonic expansions up to degree and order 25,
 120 one for each of the magnetic field components in the VFM magnetometer frame,
 121 with the position of the Sun with respect to the spacecraft parameterised by the
 122 Sun incidence angles α and β . It takes the form

$$\delta\vec{B}_{\text{Sun}} = \sum_{n=0}^{25} \sum_{m=0}^n (\vec{u}_n^m \cos m\alpha + \vec{v}_n^m \sin m\alpha) P_n^m(\sin \beta)$$

123 where \vec{u}_n^m and \vec{v}_n^m are the spherical harmonic expansion coefficients, with one com-
 124 ponent for each component of the disturbance field, and P_n^m are the Schmidt semi-
 125 normalized Legendre functions. Note that $\delta\vec{B}_{\text{Sun}}$ includes static terms ($n = m = 0$),
 126 that describe a static (i.e. independent of the Sun position) disturbance vector.
 127 The disturbance field vector $\delta\vec{B}_{\text{Sun}}$ is thus described by $3 \times 26^2 = 2,028$ model
 128 coefficients.

129
 130 The model for re-scaling the vector measurements and taking into account any
 131 small adjustment of the non-orthogonality of the VFM sensors, which is required in
 132 order to obtain the fully calibrated and corrected vector field measurements \vec{B}_{VFM} ,
 133 now takes the form

$$\vec{B}_{\text{VFM}} = \underline{\underline{P}}^{-1} \underline{\underline{S}}^{-1} \vec{B}_{\text{pre-flight}} - \delta\vec{B}_{\text{Sun}}$$

134 where $\vec{B}_{\text{pre-flight}}$ are the VFM measurements calibrated using the pre-flight param-
 135 eters and corrected for the pre-flight determined stray fields as described in [Tøffner-
 136 Clausen \(2015\)](#). $\underline{\underline{S}}$ is a 3×3 diagonal scaling matrix with elements

$$s_j = s^{\text{B-spline}}(t) + s_{j, T_{\text{sensor}}} T_{\text{sensor}} + s_{j, \beta} \beta$$

137 where $s^{\text{B-spline}}(t)$ is a quadratic B-spline in time with 3-month knot separation
 138 (common for all three components of the magnetic field), and $s_{j, T_{\text{sensor}}}$, $j = 1 - 3$
 139 is an adjustment of the pre-flight estimated dependency of the VFM sensitivity on
 140 its sensor temperature, T_{sensor} , for each sensor axis j . $s_{j, \beta}$ is an empirical scaling
 141 parameter and β the Sun incidence angle, as defined above. The choice of quadratic
 142 B-splines with 3-month knot separation is made to allow sufficient flexibility of the
 143 model; **the exact choice of B-spline knot times is not crucial as very similar results**
 144 **are obtained with other, similar parameterisations**. The estimated B-splines exhibit
 145 very moderate accelerations (in the case of the full model, see Fig. 6) and it may be
 146 possible to simplify the parameterisation of the time-dependence in future models,
 147 **e.g. to an exponential saturation in time as this is the expected behaviour of the**
 148 **VFM instrument sensitivity, however an exponential model is ill-conditioned on the**
 149 **timespan of data used here.**

150
 151 $\underline{\underline{P}}$ is the non-orthogonality matrix that makes small adjustments to the pre-flight
 152 estimated non-orthogonalities of the VFM sensor (cf. [Olsen et al., 2003](#))

$$\underline{\underline{P}} = \begin{pmatrix} 1 & 0 & 0 \\ -\sin u_1 & \cos u_1 & 0 \\ \sin u_2 & \sin u_3 & \sqrt{1 - \sin^2 u_2 - \sin^2 u_3} \end{pmatrix}$$

153 Our in-flight calibration model comprises 18 parameters in all; together with the
 154 2,028 parameters describing $\delta\vec{B}_{\text{Sun}}$ this results in 2,046 model parameters to be
 155 estimated, as listed in Table 1.

156 2.2 Estimation of Model Parameters: Inversion and Regularisation

157 In order to estimate the 2,046 model parameters from the scalar residuals we need
 158 to solve a nonlinear inverse problem. The nonlinearity arises from the ~~the~~ treatment
 159 of non-orthogonalities (*Olsen et al., 2003*).

160
 161 The forward relationship between the vector of the scalar residuals, \mathbf{d} , ($d_i = \Delta F_i$,
 162 the scalar residual of the i th data point) and the model parameter vector \mathbf{m} , may
 163 therefore be written in the form

$$\mathbf{d} = \mathbf{g}(\mathbf{m}) + \mathbf{e}$$

164 where $\mathbf{g}(\mathbf{m})$ is a nonlinear function of the models parameters and \mathbf{e} is a small re-
 165 mainder, that cannot be explained by the model, which we seek to minimise.

166
 167 Linearisation of this problem is straightforward. A *regularized, iteratively-*
 168 *reweighted, least squares solution* to the inverse problem, is then obtained using
 169 the algorithm

$$\mathbf{m}_{k+1} = \mathbf{m}_k + (\underline{\underline{\mathbf{G}}}_k^T \underline{\underline{\mathbf{W}}}_k \underline{\underline{\mathbf{G}}}_k + \lambda \underline{\underline{\mathbf{R}}})^{-1} \left(\underline{\underline{\mathbf{G}}}_k^T \underline{\underline{\mathbf{W}}}_k [\mathbf{d} - \mathbf{g}(\mathbf{m})] - \lambda \underline{\underline{\mathbf{R}}}\mathbf{m}_k \right)$$

170 where at the k th iteration, $\underline{\underline{\mathbf{G}}}_k = \left. \frac{\partial \mathbf{g}(\mathbf{m})}{\partial \mathbf{m}} \right|_{\mathbf{m}=\mathbf{m}_k}$, is the appropriate Jacobian ma-
 171 trix, $\underline{\underline{\mathbf{R}}}$ is a regularization matrix discussed in detail below, and $\underline{\underline{\mathbf{W}}}_k$ is a (Huber)
 172 weighting matrix.

173 $\underline{\underline{\mathbf{W}}}_k$ ~~is are~~ updated at each iteration, and consists of diagonal elements

$${}^k w_i = \min \left(1, \frac{c\sigma}{{}^k d_i} \right).$$

~~${}^k d_i$ is the scalar residual of the i th data point using model vector \mathbf{m}_k , $\Delta F_i = \left| \vec{B}_{i,\text{VFM}} \right| - F_{i,\text{ASM}}$
 is the scalar residual of the i th data point, with $\vec{B}_{i,\text{VFM}}$ calculated using the model
 parameters from iteration k , and F_{ASM} being the fully calibrated and corrected
 scalar field measurements from the ASM scalar magnetometer, and~~

$$\sigma = \sqrt{\frac{\sum_i ({}^{k-1} w_i {}^k d_i)^2}{\sum_i {}^{k-1} w_i^2}},$$

174 being a (robust) estimate of the standard deviation of the residuals at iteration k .
 175 We set $c = 2$, slightly higher than the value of 1.5 usually chosen, in order to ensure
 176 that the less numerous polar data are not overly downweighted in the determination
 177 of the calibration parameters.

178

179 It turns out that the full set of 2,046 parameters is not needed to obtain good re-
 180 sults and low data misfit, which is confirmed by inspection of the eigenvalues of the
 181 matrix $(\underline{\mathbf{G}}_k^T \underline{\mathbf{W}}_k \underline{\mathbf{G}}_k + \lambda \underline{\mathbf{R}})$, as presented in Fig. 4 for *Swarm Alpha*. The magnitudes
 182 of the sorted eigenvalues (in order of decreasing magnitude) exhibit a distinct drop
 183 around 750-800 degrees of freedom, indicating the smaller eigenvalues contribute
 184 little to the solution. The inversion of this matrix was therefore finally performed
 185 using a truncated singular value decomposition (TSVD) procedure, retaining only
 186 750 degrees of freedom.

187

188 A regularization matrix $\underline{\mathbf{R}}$ is also included to help ~~stabilizeto~~ **stable** the inver-
 189 sion. This is necessary because the *Swarm* satellites operates in a tightly controlled
 190 attitude orientation which leads to a poor excitation of the VFM instrument along
 191 the axis perpendicular to the orbit plane (the East-West direction corresponding
 192 to the y -axis of the VFM sensor). Consequently, the parameters related to the y -
 193 axis are poorly determined in a scalar calibration. The regularization matrix $\underline{\mathbf{R}}$ is
 194 therefore defined so that it acts on the parameters $s_{2,\text{Tsensor}}$, $s_{2,\beta}$, u_1 , and u_3 to
 195 force $s_{2,\text{Tsensor}} \simeq (s_{1,\text{Tsensor}} + s_{3,\text{Tsensor}}) / 2$ (to reflect the physical properties of the
 196 VFM sensor) and also to minimize the norms $s_{2,\beta}^2$ and $u_1^2 + u_3^2$. λ is chosen to be
 197 sufficiently large to effectively impose the regularisation on the estimated model.
 198 Note that no regularisation is directly imposed on $\delta \vec{B}_{\text{Sun}}$ but use of truncated SVD
 199 during the inversion automatically acts to suppresses structure in regions that are
 200 not well constrained by the input data.

201

202 The starting model for the inversions is “unity”, i.e. $\underline{P} = \underline{S} = \underline{I}$, where \underline{I} is
 203 the identity matrix, and $\vec{u}_n^m = \vec{v}_n^m = \vec{0}$. The inversions typically converge within
 204 25 iterations.

205 3 Results of Model Estimation for Swarm Alpha

206 The model described above is estimated for *Swarm Alpha* using data from the begin-
 207 ning of the mission (22 November 2013) until June 2015. Fig. 1 shows the final scalar
 208 residuals, i.e. the residuals after application of the model (after “calibration and
 209 correction”) of the VFM measurements, (in green) as a function of time together
 210 with the residuals of the un-corrected but re-scaled vector field measurements, i.e.
 211 $\vec{B}_{\text{VFM}} + \delta \vec{B}_{\text{Sun}}$, in light blue; these data illustrate what can be achieved with the
 212 traditional scalar calibration methods. Note the excellent reduction of the scalar
 213 residuals achieved by the model; the Huber weighted rms of the residuals drops
 214 from 963 pT to 168 pT. Table 2 provides the corresponding numbers for *Bravo* and
 215 *Charlie*.

216

217 Fig. 5 shows normal distribution plots for the scalar residuals. The top plot shows
 218 the distributions of all data for un-corrected (red) and fully corrected data (green)

219 and demonstrates a transition from a non-Gaussian to Gaussian residual distri-
 220 bution when applying the model. The bottom plots show the distributions of the
 221 data split into 3-months periods, un-corrected to the left and corrected to the right.
 222 These also demonstrate the elimination of systematic and non-Gaussian effects.

223

224 Table 3 lists the estimated s_{Tsensor} and s_{β} parameters, and the non-orthogonality
 225 values for all three *Swarm* satellites together with their estimated pre-flight values
 226 for the VFM instrument itself for reference. I.e. the table shows the adjustments
 227 applied in order to reduce the scalar residuals to the level indicated above.

228

229 Table 4 shows the increase in the weighted rms of the scalar residuals when omit-
 230 ting individual parts of the model – a full re-estimation of the remaining model
 231 parameters is carried out for each table entry. Particularly the omission of the non-
 232 orthogonalities drastically increases the misfit – the power (the mean-square) is
 233 more than doubled. Due to the stable attitude of the *Swarm* satellites, the small
 234 x - z non-orthogonality angle, u_2 , is equivalent to first order to a small, relative
 235 timeshift between the ASM and VFM measurements – 1 arc-second corresponds
 236 roughly to a 3 ms timeshift, and it has been discussed whether it would be more
 237 reasonable to introduce such timeshifts rather than adjusting the pre-flight esti-
 238 mated non-orthogonalities. However, the variations in the u_2 angles estimated by
 239 this model would imply time-shifts varying from -3 ms to $+13$ ms for the individual
 240 satellites which, to the authors, seems quite unlikely.

241

242 The temporal evolution of the scaling of the vector field measurements, $s^{B-spline}$,
 243 is shown in Fig. 6 for the various test models listed in Table 4. The full model, shown
 244 in redgreen, shows a smooth behaviour in time, as expected from an instrument
 245 design perspective. The blue curve shows the model without s_{β} ; this exhibits some
 246 small oscillations, whereas the light brownred (no s_{Tsensor}) and greenmagenta (no
 247 $\delta\vec{B}_{\text{Sun}}$) curves show much higher level of oscillations indicating they are inadequate
 248 to capture the behaviour of the measurements. The elimination of the oscillations
 249 in the full model is a good indicator of the validity of this model. The magentaeyan
 250 curve shows the model without non-orthogonalities; this is rather close to the curve
 251 of the full model and indicates the decoupling of the non-orthogonalities from any
 252 long-term temporal effect of the measurement disturbances and instruments.

253

254 Maps of the three components of the estimated disturbance fields from the full
 255 model as function of Sun incidence angles α (abscissa) and β (ordinate) are given
 256 in Figs. 7, 8, and 9 for *Swarm Alpha*, *Bravo*, and *Charlie* respectively. During nomi-
 257 nal flight, the Sun incidence angles traverse these plots horizontally from right
 258 to left, and move up or down in β as the orbit plane moves through local time.
 259 The Sun induced disturbance is observed to have temporal characteristics that are
 260 observed in the plots as horizontally stretched features, these are attributed to
 261 thermal capacitance: The Sun induced disturbance exhibits characteristic warm-up
 262 and cool-down effects, i.e. the disturbance increases when the spacecraft is exposed
 263 to the Sun, and decreases when the Sun exposure terminates. The time constants
 264 for these effects are up to tens of minutes (corresponding to several tens of degrees

265 in the α angle). This effect is captured by the spherical harmonic model expansion
266 of $\delta\vec{B}_{\text{Sun}}$ and yields the horizontally stretched features in Figs. 7-9. Note also the
267 regions of nightside data (eclipse), the circled areas to the left of the figures, which
268 generally show less disturbance; this is not imposed by the model or any regulari-
269 sation, rather it is simply a result of the data itself, and thus another indicator of
270 the ability of the model to describe the observed disturbances. The plots also show
271 both the similarities and the differences in $\delta\vec{B}_{\text{Sun}}$ between the three satellites.

272

273 4 Conclusions

274 We have established a predominantly empirical model for the calibration and cor-
275 rection of the magnetic vector field measurements of the three *Swarm* spacecraft.
276 The model is based on detailed studies of the observed scalar residuals between the
277 measurements of the absolute scalar magnetometer, ASM, and the modulus of the
278 measurements of the vector field magnetometer, VFM. The model has proven to be
279 quite robust as more data are incorporated into the estimation of the model paramete-
280 rs, although the ambiguity of determining vector disturbances from a pure scalar
281 calibration affects the estimated correction vectors; these corrections do change
282 slightly (by a few tenths of a nT) as more data are added.

283

284 The estimated models reduce the scalar differences between the *Swarm* magne-
285 tometers to generally below 0.5 nT with rms values well below 200 pT for all three
286 satellites, and have been in operational use since April 2015 to produce corrected
287 *Swarm* Level 1b magnetic field vector data (as of version 0401).

288

289 Future evolutions of the model presented here are foreseen to include changing
290 the model of the temporal evolution of the VFM sensitivity from B-splines to an
291 exponentially decaying function. Analysis of $\delta\vec{B}_{\text{Sun}}$ also indicates that this vector is
292 generally confined to a few, distinct directions which may be incorporated in future
293 models. Finally, it may be possible to model the effect of the thermal capacitance
294 using appropriate temporal filter functions which would lead to a significant reduc-
295 tion of the number of parameters of the model.

296

297 *Data Availability*

298 The estimated disturbance vectors, $\delta\vec{B}_{\text{Sun}}$, are included in the operational Level 1b
299 magnetic *Swarm* data products as `dB_Sun`.

300

301 Uncorrected data are available at <ftp://swarm-diss.eo.esa.int/Advanced/> (login
302 required, access can be requested via <https://earth.esa.int/Swarm>).

303

304 **Competing interests**

305 The authors declare that they have no competing interests.

306 **Author's contributions**

307 LTC carried out the in-flight scalar calibration and characterisation, analysed the results, and led the writing of this
308 manuscript. VL proposed the model for the Sun induced vector disturbance, $\delta\vec{B}_{\text{Sun}}$, and made the first estimations
309 using this model. NiO and CF supported the entire project with many discussions, suggestions, and source code.

Acknowledgements

We would like to thank ESA for establishing and providing support to the ASM-VFM Task Force with the aim of investigating the source of the scalar residuals observed in the *Swarm* magnetic measurements, and developing a correction scheme. We would also like to thank this Task Force for its work in characterising the behaviour of the magnetic disturbance and for many fruitful discussions and inputs for this work. In particular, we would like to thank Peter Brauer from the VFM instrument team for detailed discussions on the modelling and on the characteristics of the VFM instruments. **Two anonymous reviewers are thanked for their comments that helped to improve the clarity of the manuscript.** This paper is the IGP contribution XXXX.

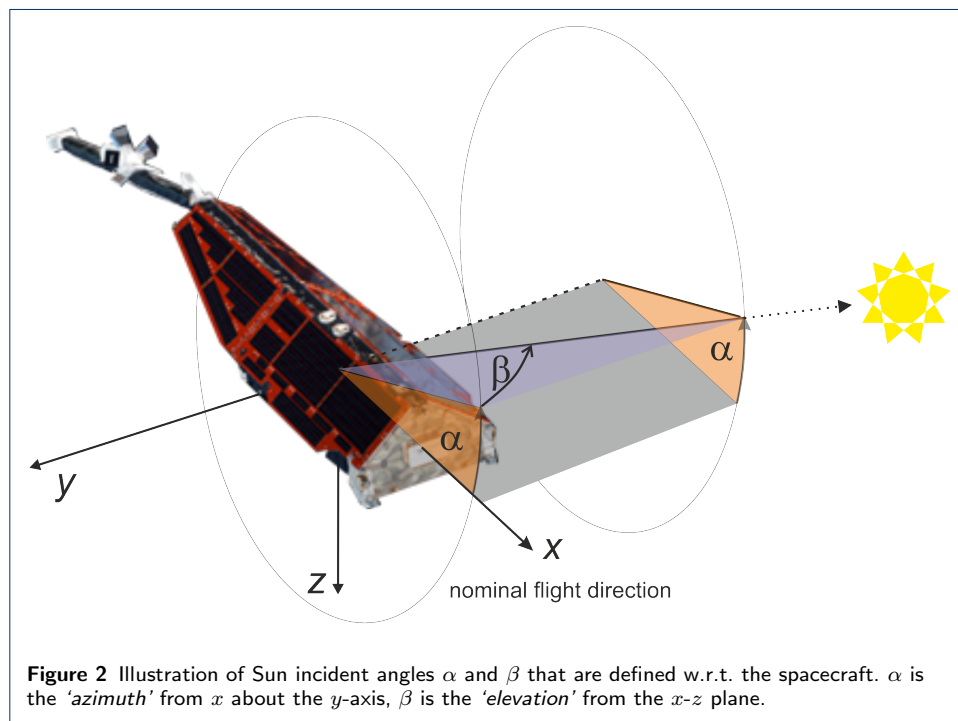
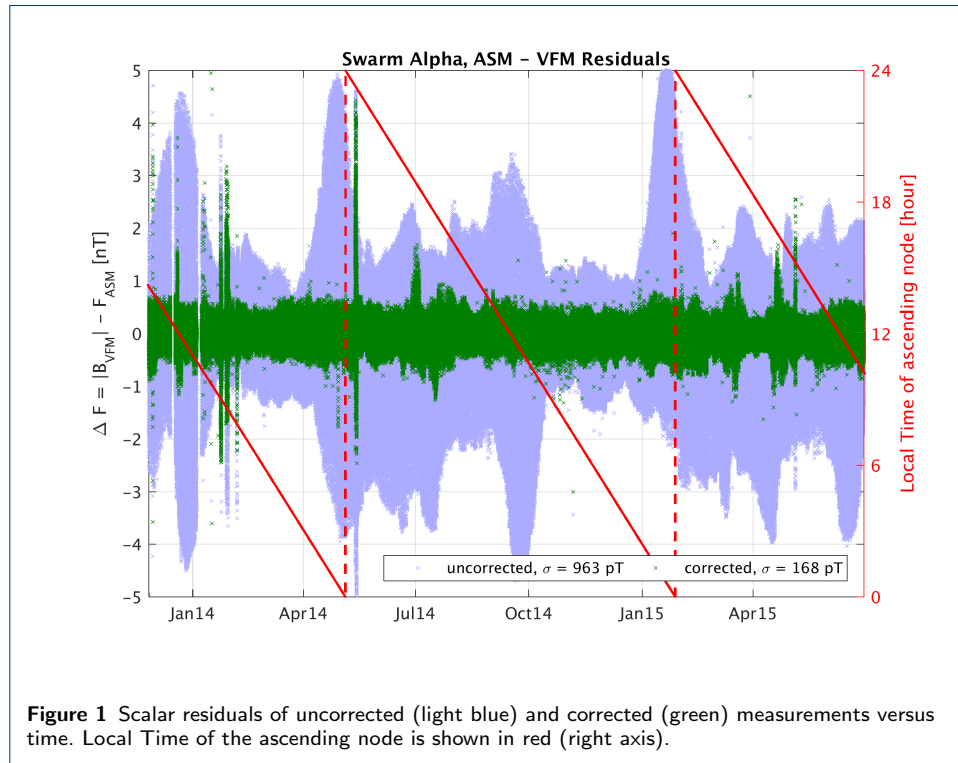
Author details

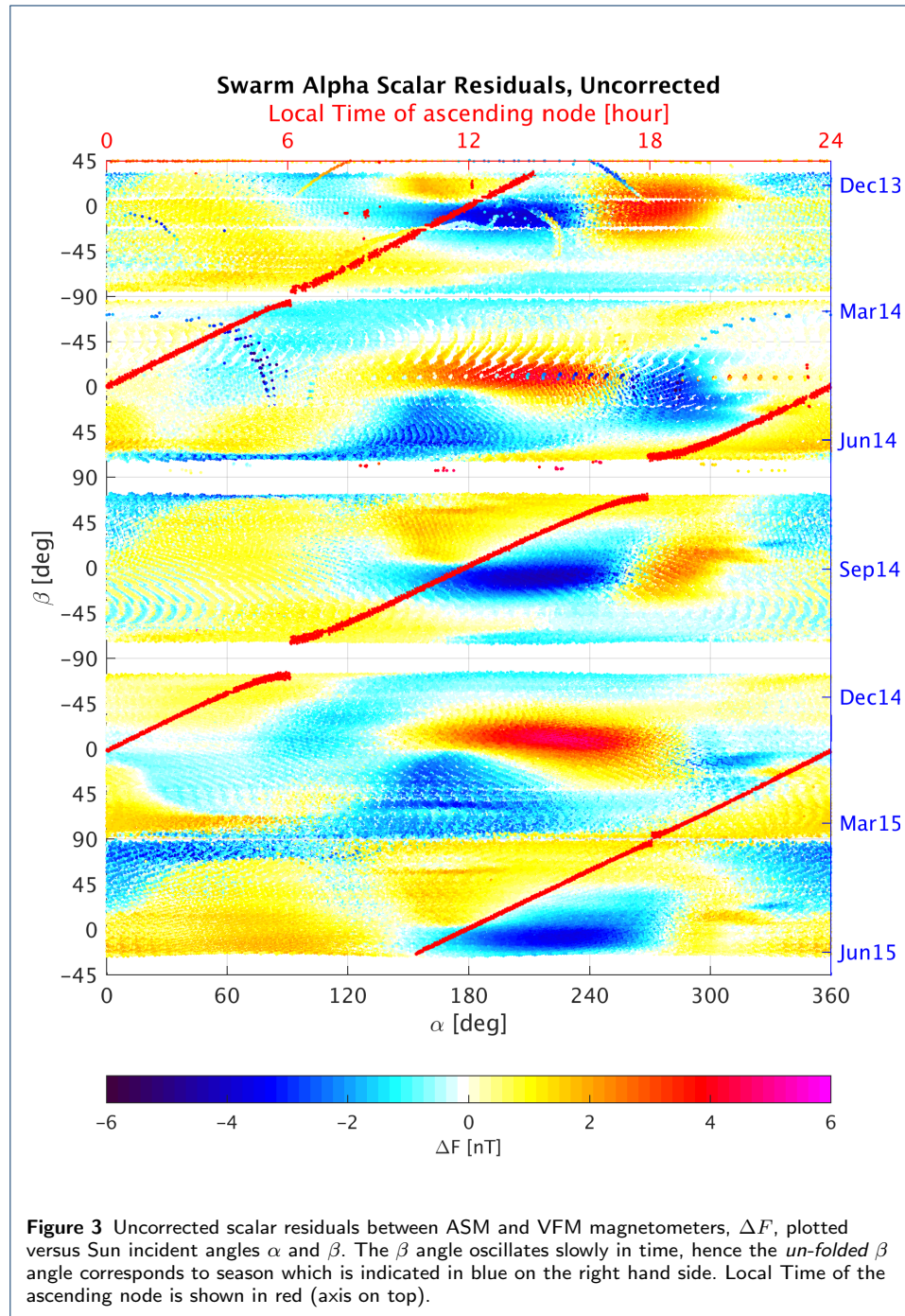
¹Division of Geomagnetism, DTU Space, Technical University of Denmark, Diplomvej, Kongens Lyngby, Denmark
.
²National Magnetic Observatory Geomagnetism, Institut de Physique du Globe de Paris, 1 rue Jussieu, Paris, France
.
.

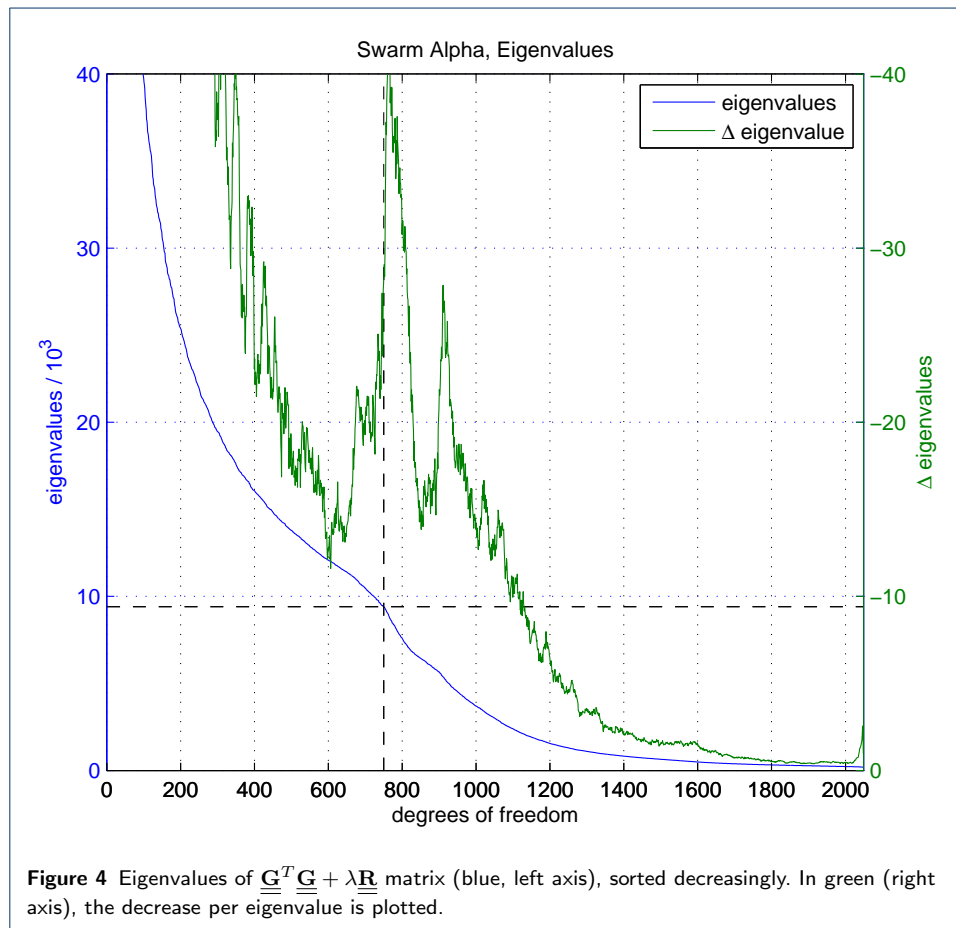
References

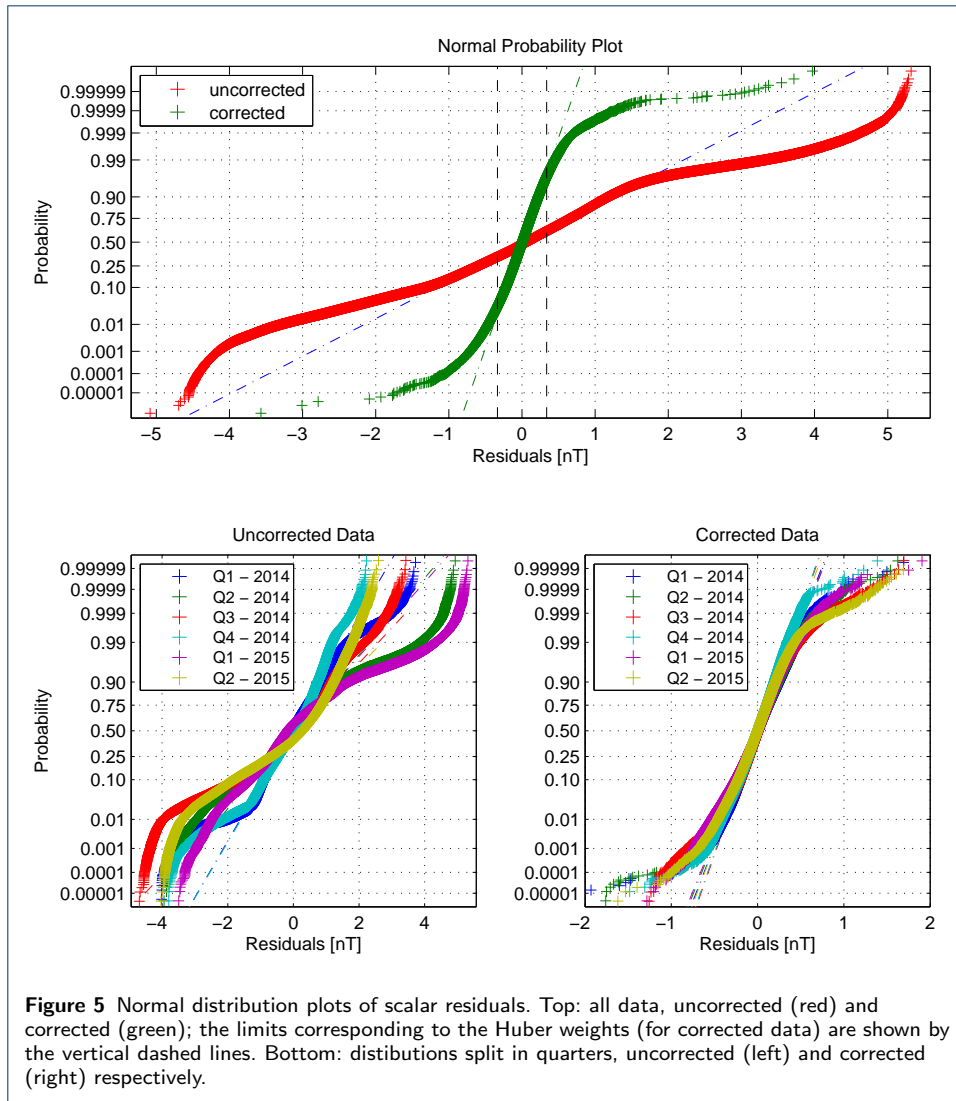
- Floberghagen, R., et al. (2016), The Swarm mission - an overview two years after launch, *Earth, Planets and Space*.
Friis-Christensen, E., H. Lühr, and G. Hulot (2006), *Swarm: A constellation to study the Earth's magnetic field*, *Earth, Planets and Space*, 58, 351–358.
Lesur, V., M. Rother, I. Wardinski, R. Schachtschneider, M. Hamoudi, and A. Chambodut (2015), Parent magnetic field models for the IGRF-12 GFZ-candidates, *Earth, Planets and Space*, 67(1), .
Olsen, N., et al. (2003), Calibration of the Ørsted vector magnetometer, *Earth, Planets and Space*, 55, 11–18.
Tøffner-Clausen, L. e. (2015), *Swarm* level 1b processor algorithms, *Esa doc. sw-rs-dsc-sy-0002*, National Space Institute, DTU Space, Copenhagen.
Yin, F., and H. Lühr (2011), Recalibration of the CHAMP satellite magnetic field measurements, *Measurement Science and Technology*, 22(5), 055,101, .

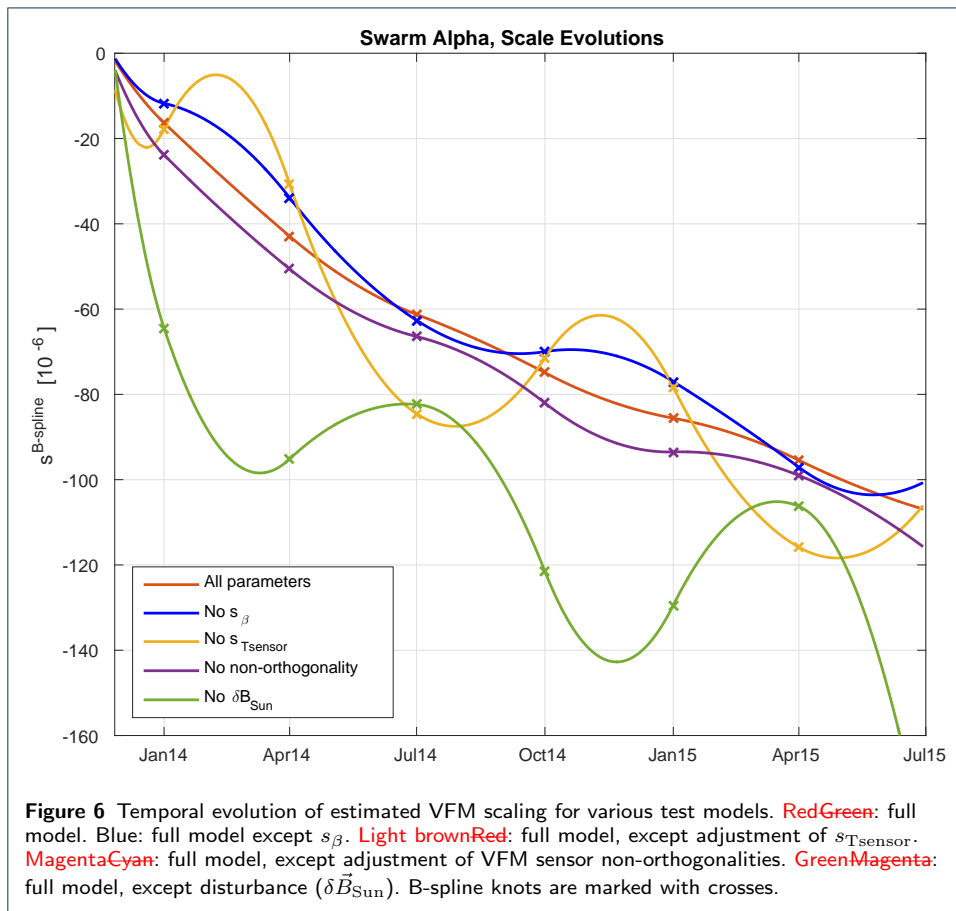
335 Figures

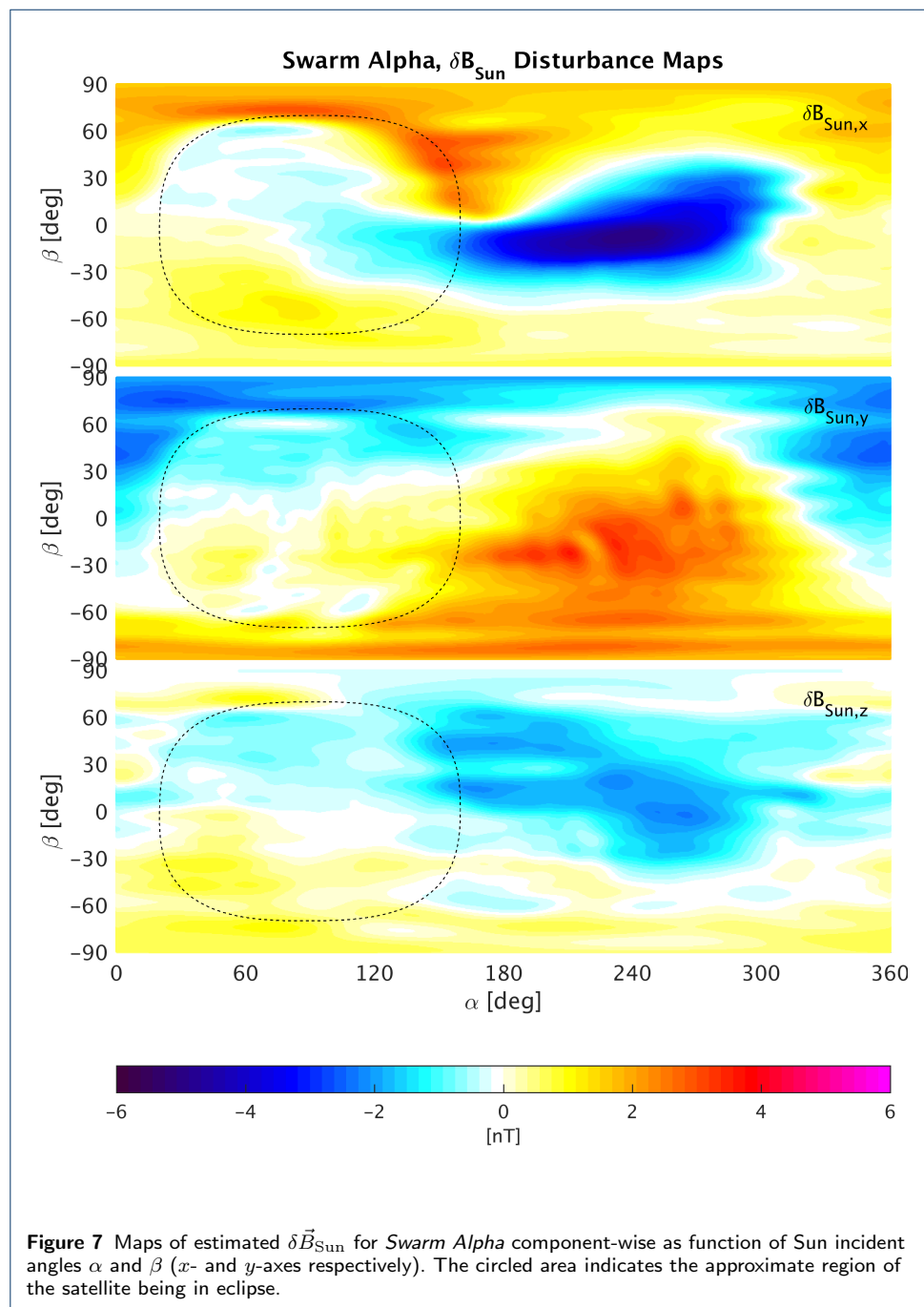


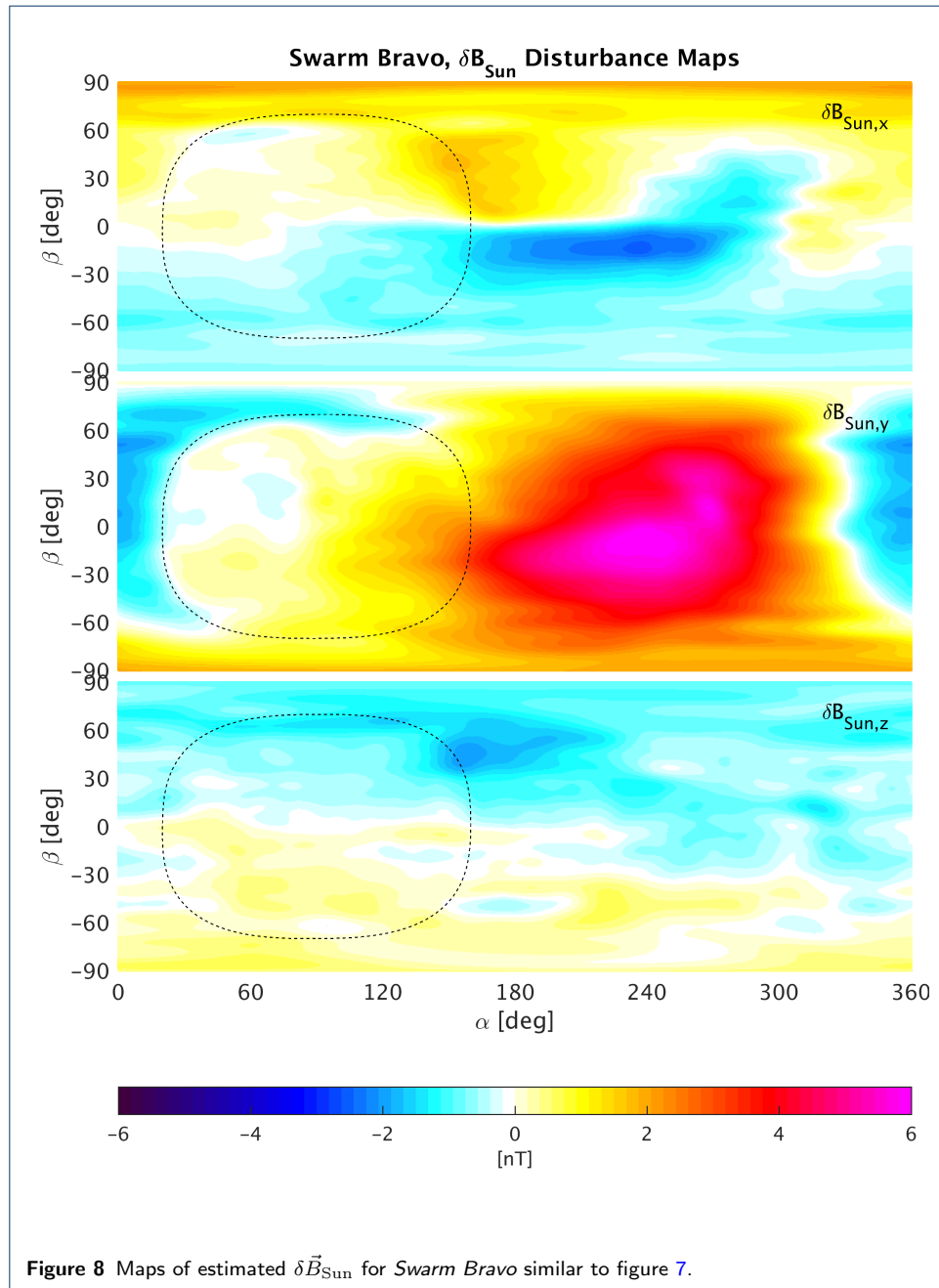


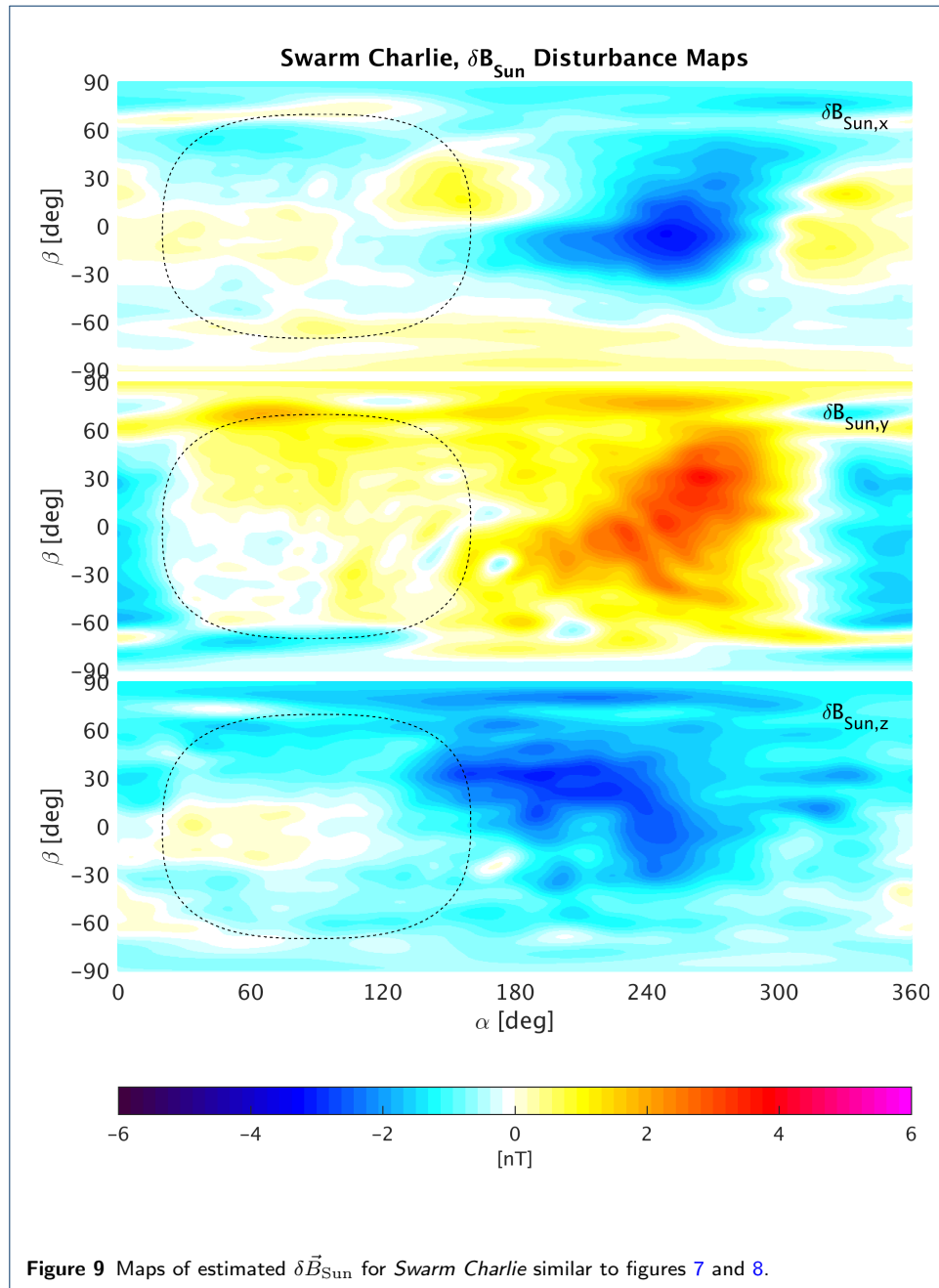












336 Tables

Table 1 Model parameters

Description	Parameters	Dimension
$\delta \vec{B}_{\text{Sun}}$	\vec{u}, \vec{v}	2,028
Sensitivity, time dependent	$s^{B\text{spline}}$	9
Sensitivity, β dependency	\vec{s}_{β}	3
Sensitivity, sensor temperature dependency	$\vec{s}_{T\text{sensor}}$	3
Non-orthogonalities	u_1, u_2, u_3	3
Total		2,046

Table 2 Scalar Residual Statistics, Uncorrected and Corrected Data.

For *Swarm Charlie* two sets of numbers are given; one set for which the ASM was still working (F_{ASM} , until 5. November 2014) and one set using the scalar data from *Swarm Alpha* mapped to the position of *Swarm Charlie* ($F_{\text{AC,map}}$). For data from 1. May 2014 through 5. November 2014 the weighted rms of $F_{\text{ASM}} - F_{\text{AC,map}}$ is 572.6 pT.

Satellite	Weighted rms [pT]	
	Uncorrected	Corrected
<i>Alpha</i>	962.6	168.3
<i>Bravo</i>	710.3	164.2
<i>Charlie</i> F_{ASM}	632.1	172.3
$F_{\text{AC,map}}$	862.1	527.7

Table 3 Estimated values for selected model parameters for all three *Swarm* satellites. The nT -equivalents of the adjustments in a 50,000 nT ambient field are: $s_{T\text{sensor}} = 10^{-6}/^{\circ}\text{C} \sim 1.25 nT$ (25°C temperature swing), $s_{\beta} = 0.1 \times 10^{-6}/\text{deg} \sim \pm 0.45 nT$ (± 90 deg), $u = 1$ arc-second $\sim 0.242 nT$.

Sat	Sensitivity/sensor temperature, $s_{T\text{sensor}}$, [$10^{-6}/^{\circ}\text{C}$]		Sensitivity/ β angle, s_{β} , [$10^{-6}/\text{deg}$]		Non-orthogonalities, $u_{1,2,3}$, [arc-seconds]	
	Pre-flight	Adjustment	Pre-flight	Adjustment	Pre-flight	Adjustment
<i>Alpha</i>	28.5	0.616	–	-0.125	102.386	-0.601
	28.8	0.780	–	0	217.403	-3.960
	28.3	0.945	–	0.012	-179.318	0.149
<i>Bravo</i>	28.3	1.168	–	-0.132	350.880	-0.558
	29.0	1.385	–	-0.003	62.432	-2.453
	28.8	1.602	–	-0.198	-147.060	1.608
<i>Charlie</i>	27.7	1.521	–	-0.090	139.140	0.094
	29.1	1.300	–	-0.038	-248.890	1.042
	28.4	1.076	–	-0.167	-109.960	0.805

Table 4 Weighted rms values for various models, *Swarm Alpha*

Model	weighted rms [pT]	Residual power (normalized)
Full model	168.3	100%
No s_{β}	176.1	107%
No $s_{T\text{sensor}}$	181.7	116%
No non-orthogonalities	250.2	221%
No $\delta \vec{B}_{\text{Sun}}$	962.6	3,269%